The WW domain of IQGAP1 binds directly to the p110α catalytic subunit of PI 3-kinase

by A. Jane Bardwell[1], Maria D. Andrade-Ludeña[1], Kiku C. Yoneda[1], Oanh T. Nguyen[1], David A. Fruman[2], and Lee Bardwell[1,3]

[1]Dept. of Developmental and Cell Biology, University of California, Irvine, CA, USA

[2]Dept. of Molecular Biology and Biochemistry, University of California, Irvine, CA, USA

[3]Corresponding author: bardwell@uci.edu

Running Title: IQGAP1 WW domain binds to PI3K p110α

Keywords:
Scaffold
PI3K
Phosphoinositide
Signaling
Cancer

Abstract

IQGAP1 is a multi-domain cancer-associated protein that serves as a scaffold protein for multiple signaling pathways. Numerous binding partners have been found for the calponin homology, IQ and GAP-related domains in IQGAP1. Identification of a binding partner for its WW domain has proven elusive, however, even though a cell-penetrating peptide derived from this domain has marked anti-tumor activity. Here, using *in vitro* binding assays with human proteins, we show that the WW domain of human IQGAP1 binds directly to the p110α catalytic subunit of phosphoinositide 3-kinase (PI3K). In contrast, the WW domain does not bind to ERK1/2, MEK1/2, or the p85α regulatory subunit of PI3K when p85α is expressed alone. However, the WW domain is able to bind to the p110α/p85α heterodimer when both subunits are co-expressed, as well as to the mutationally activated p110α/p65α heterodimer. We present a model of the structure of the IQGAP1 WW domain, and experimentally identify key residues in the hydrophobic core and beta strands of the WW domain that are required for binding to p110α. These findings contribute to a more precise understanding of IQGAP1-mediated scaffolding, and of how IQGAP1-derived therapeutic peptides might inhibit tumorigenesis.

Introduction

Recently there has been renewed enthusiasm for targeting protein-protein interactions as a therapeutic strategy for treating cancer and other diseases, and for using peptide-based inhibitors as drugs or drug leads in such approaches [1-11]. Signaling scaffold proteins – large, multidomain proteins that bind to multiple members of one or more signaling pathways – participate in numerous protein-protein interactions that could be targeted to disrupt signaling [7, 12-16]. Indeed, studies with human IQGAP1, a scaffold protein for multiple cancer-associated signaling pathways [17-21], have led to the discovery that its 27-residue WW domain, when engineered as a cell-penetrating peptide, shows broad anti-tumor activity with minimal associated toxicity [12, 22].

WW domains are one of the smallest independently folding protein interaction domains, and thus have a strong potential as leads in peptidomimetic development. These domains are typically between 27 and 35 residues in length and fold into a three-stranded antiparallel beta-sheet [23-25]. WW domains are characterized as proline recognition domains, and typically bind to proline-rich short linear motifs in their binding partners [26]. A cell-penetrating derivative of the IQGAP1 WW domain was first developed by Jameson *et al*. [12], who showed that this peptide inhibited the proliferation, migration, viability and tumor-forming ability of breast, colorectal and melanoma tumor cells that contained activating mutations in the RAS/MAPK pathway. Non-transformed or primary cells were unaffected. They further showed that the WW peptide, when delivered systemically, significantly increased the lifespan of mice bearing pancreatic tumors [12]. Choi *et al*. [22] showed that the WW peptide reduced the viability of multiple additional breast cancer cell lines, but did not adversely affect normal control lines. The anti-tumor activity of the WW peptide has also been confirmed in other studies [27, 28].

In view of these exciting results, it is imperative to determine the binding partner(s) of the WW domain. For many years, it was believed that the ERK1 and ERK2 MAP kinases bound to the WW domain of IQGAP1, and were the only proteins to do so [29-31]. Indeed, this belief motivated the Jameson *et al*. study, as these workers sought to target ERK signaling. In 2017, however, we showed that ERK1 and ERK2 do not bind to IQGAP1's WW domain, but instead bind to the nearby IQ domain [32]. This finding revived the search for the authentic target of the IQGAP1 WW domain.

A significant clue in this regard came from a landmark 2016 study from the Anderson lab [22]. These authors showed that IQGAP1 acts a scaffold protein for the phosphoinositide 3-kinase (PI3K) pathway by binding to several enzymes that modify phosphoinositides, including PI3K itself. PI3Ks are a family of enzymes that phosphorylate inositol lipids in response to signals from growth factors, cytokines, and other cellular and environmental cues. In so doing, they regulate cell proliferation, growth, survival, motility, intracellular trafficking, and metabolism [33-37]. The most common PI3K isoform is a heterodimer of a catalytic subunit designated p110α (gene *PIK3CA*) and a regulatory subunit designated p85α (gene *PIK3R1*). Following activation by growth factors, insulin, or other signals, the p110α/p85α holoenzyme phosphorylates the inositol ring of phosphatidylinositol-(4,5)-biphosphate (PIP2) on the 3-position to generate phosphatidylinositol-(3,4,5)-triphosphate (PIP3), a key intracellular second messenger. Both subunits of PI3K, particularly p110α, are recognized oncogenic drivers that are frequently mutated in human cancer and tissue overgrowth syndromes. In addition to being activated by direct mutation, PI3K activity can also be pathologically activated by other means, including mutations in other oncogenes, loss of tumor suppressor genes (especially the PTEN tumor suppressor), and oncovirus-mediated transformation [33-37]. Hence, PI3K activation is a hallmark of cancer [35].

Here, we show that the WW domain of human IGQAP1 binds directly to human p110α protein, the catalytic subunit of the PI3K holoenzyme. We also present a model of this WW domain, and investigate which residues in the domain participate in the interaction with p110α. These findings contribute to a more precise understanding of IQGAP1-mediated scaffolding, and of how IQGAP1-derived therapeutic peptides might inhibit tumorigenesis.

Results

The WW domain of IQGAP1 binds specifically to p110α

Although IQGAP1 had been shown to act as a scaffold protein for the PI 3-kinase pathway [22] and the RAS/RAF/MEK/ERK pathway [29, 32], the precise binding partner of IQGAP1's WW domain was unknown. We took a "candidate protein" approach to finding this partner, using components from both of these pathways. First, the WW domain of human IQGAP1 (residues 684-710, Figure 1A) was fused at its N terminus to *Schistosoma japonicum* glutathione *S*-transferase (GST), and the resulting fusion protein (GST-WW) was expressed in bacteria and purified by adsorption to glutathione-Sepharose beads. Next, GST-WW (or GST alone as a negative control) was incubated with full-length human p85α or p110α that had been produced in radiolabeled form by *in vitro* translation (Figure 1B). We also assessed the ability of GST-WW to bind to *in vitro*-translated human ERK2 proteins (Figure 1B). Bead-bound complexes were collected by sedimentation, washed extensively, and analyzed by SDS-PAGE and autoradiography. As shown in Figure 1C, full-length p110α bound efficiently to WW, but p85α did not. Furthermore, the binding was specific, because only trace precipitation of p110α occurred when GST was used instead of the GST-WW fusion protein. GST-WW did not exhibit detectable binding to human ERK2 (Figure 1C).

Over the course of these studies, we used two different variants of full-length human p110α protein. The first version contained an N-terminal myc-epitope tag, and the second version was the unaltered 1086-residue wild-type protein. Quantification of 12-15 independent experiments for each variant is shown in Figure 1D, and demonstrates that the presence or absence of the N-terminal myc tag did not affect the binding of GST-WW p110α. Furthermore, for both variants, their binding to GST-WW was statistically-significantly different from their binding to GST alone, with a very high level of confidence ($p < .0001$). Figure 1D also shows that for p85 and ERK2, both of which were assessed repeatedly over multiple different experiments, the trace binding to GST-WW was indistinguishable from the level of binding to GST alone ($p > .99$ for p85α, $p > .40$ for ERK2).

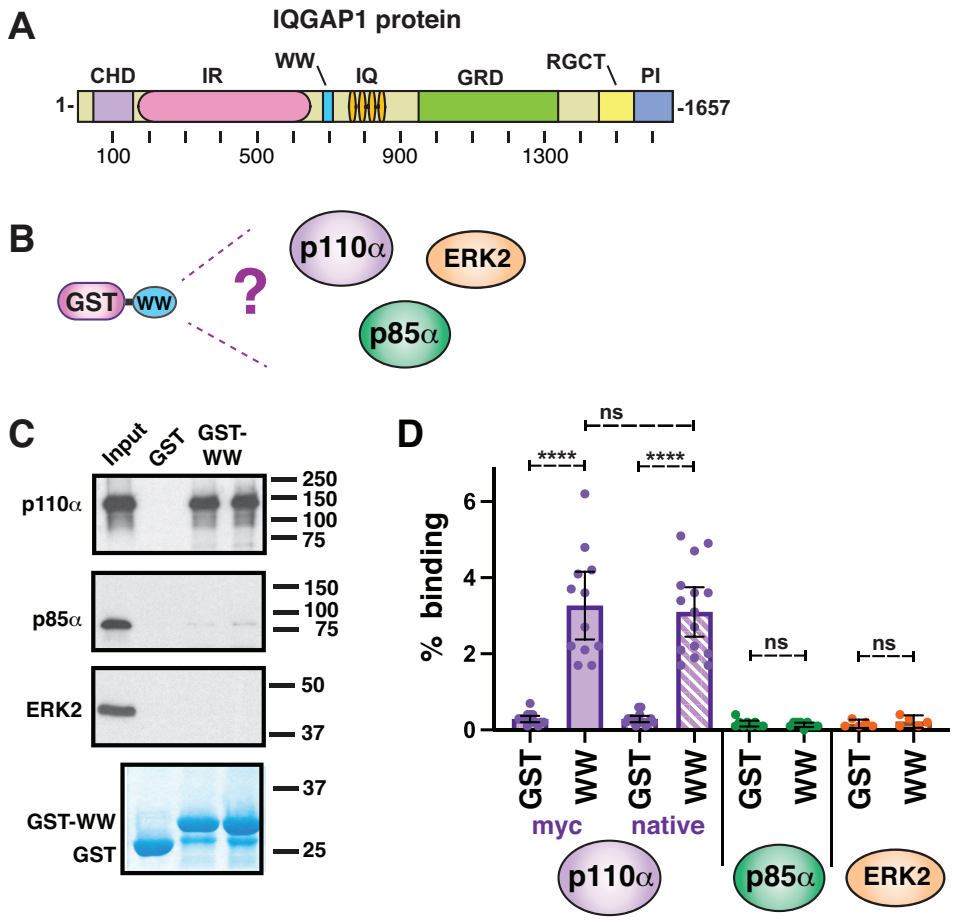

Figure 1. The WW domain of IQGAP binds to the catalytic subunit of PI 3-kinase.
(**A**) Schematic depicting full-length human IQGAP1 protein with domains denoted as follows: CHD, calponin homology domain; IR, internal repeated sequence/coiled-coil domain; WW, WW domain; IQ, IQ domain; GRD, GTPase-activating protein-related domain; RGCT, RasGAP C-terminal domain; PI, phosphoinositide binding domain.
(**B**) The WW domain of human IQGAP1, fused to GST, was tested for binding to the p110α and p85α subunits of PI3K, as well as to the ERK2 MAP kinase.
(**C**) As shown in **B**, ^{35}S-radiolabeled full-length human p110α, p85α and ERK2 proteins were prepared by *in vitro* translation and partially purified by ammonium sulfate precipitation, and portions (5% of the amount added in the binding reactions) were resolved on a 10% SDS-polyacrylamide (SDS-PAGE) gel; these samples are labeled "Input" in the figure. Portions (1 pmol) of the same proteins were incubated with 25 μg of GST or GST-WW bound to glutathione-Sepharose beads, and the resulting bead-bound protein complexes were isolated by sedimentation and resolved by10% SDS-PAGE on the same gel. The gel was analyzed by staining with a Coomassie-blue-based reagent for visualization of the bound GST fusion protein (a representative example is shown in the lowest panel) and by X-ray film exposure for visualization of the bound radiolabeled protein (upper three panels). The migration of molecular weight markers is indicated on the right. Lanes 3 and 4 are technical replicates.
(**D**) Quantification of the binding of human p110α, p85α and ERK2 proteins to GST or GST-WW. The results shown are the average of 5-15 independent repetitions of the of the type of binding assay shown in B and C (n = 12 for myc-tagged p110α, n = 15 for native p110α, n = 8 for p85α, n = 5 for ERK2). Error bars show the 95% confidence interval; individual data points are shown as dots. Technical replicates in a given experiment (e.g. lanes 3 and 4 in C) were averaged together to create a single data point. ****, $p < 0.0001$; ns, not significant ($p > 0.05$).

In addition to not binding to ERK2 (Figure 1), GST-WW also did not exhibit detectable binding to human ERK1, MEK1 or MEK2 (Figure 2 A,B). These negative results with RAS/MAPK pathway components confirmed our previously published data that used a different experimental approach to show that ERK1, ERK2, MEK1 and MEK2 all bind to the IQ domain of IQGAP1, and not to the WW domain [32]. In addition, these results demonstrated that our GST-WW construct was not non-specifically sticky.

The WW domains of some proteins bind to other regions of the same protein; these in-trans or in-cis interactions mediate homodimerization or autoinhibition [38, 39]. Hence, we also asked whether GST-WW was able to bind to full-length IQGAP1 protein, or to IQGAP1 truncations lacking the WW domain. We found no evidence for such self-interaction (Figure 2 C,D). However, it should be noted that our binding assay would not be able to detect weak, millimolar-affinity interactions that might be nevertheless be significant if driven by local concentration effects.

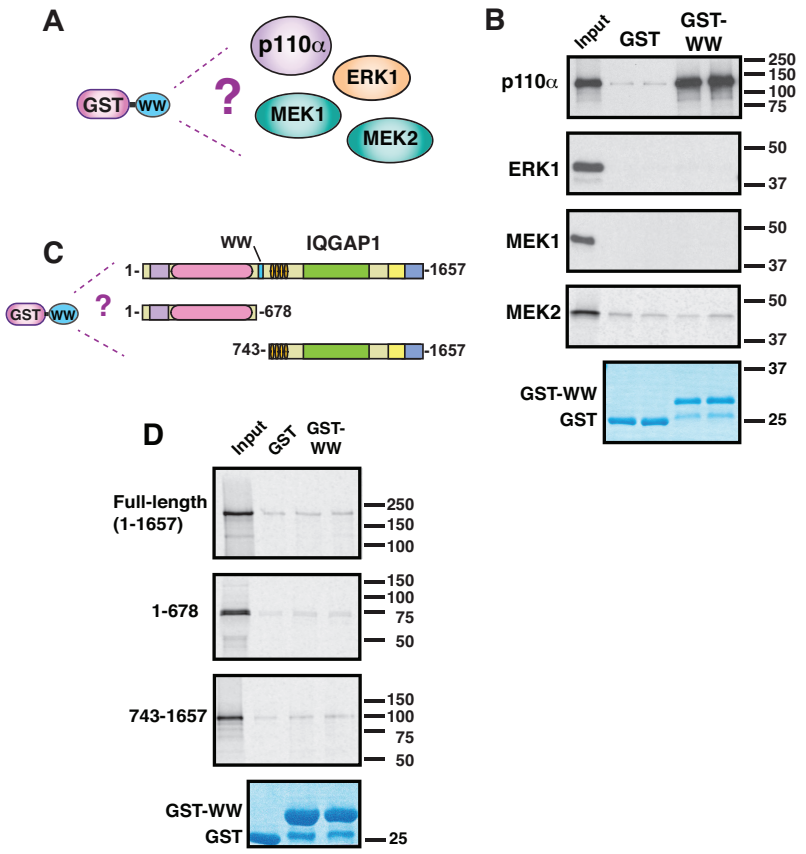

Figure 2. The WW domain of IQGAP does not bind to ERK1, MEK1, MEK2, or to IQGAP1 itself.
(**A**) The WW domain of human IQGAP1, fused to GST, was tested for binding to p110α, ERK1, MEK1 and MEK2.
(**B**) Autoradiogram of a representative experiment of binding assays described in **A**. Each binding assay shown was repeated three separate times (i.e. three independent experiments), with duplicate points (i.e. technical replicates) in each experiment. Other details as in Figure 1.
(**A**) The WW domain of human IQGAP1, fused to GST, was tested for binding to full-length human IQGAP1, as well as to the 1-678 and 743-1657 fragments of IQGAP1.
(**D**) Autoradiogram of a representative experiment of binding assays described in **C**. Other details as above.

To summarize, the experiments described in this section demonstrate that the WW domain of human IQGAP1 binds directly and specifically to the catalytic subunit of human PI 3-kinase.

The WW domain of IQGAP1 binds to the p85α/p110α complex

In cells, the majority of p110α molecules are bound to p85α in the form of p110α/p85α heterodimers, although p85α also has independent functions [40]. To ask if the WW domain of IQGAP1 could bind to p110α/p85α heterodimers, we co-translated p110α and p85α in the same *in vitro*-translation reaction, and then assessed the binding of this co-translated mix to GST-WW; p110α translated alone and p85α translated alone were included for comparison (Figure 3A). As shown in Figure 1 and in Figure 3B, p85α alone did not display detectable binding to GST-WW, whereas p110α bound efficiently. Nevertheless, p85α co-translated with p110α bound to GST-WW (Figure 3B, see also Supplementary Figure 1). Indeed, the results, when quantified and corrected for labeling efficiency, indicated that there was an approximately 1:1 molar ratio of p85α to p110α in the bound fraction (see Figure 3B legend for quantification). This experiment demonstrates that the WW domain of IQGAP1 is able to bind to p110α/p85α heterodimers as well as to p110α monomers.

In the p110α/p85α heterodimer, the catalytic activity of p110α is repressed by p85α, but this repression is relieved when the two SH2 domains in p85α bind to phosphotyrosine residues on receptor tyrosine kinases or adaptor proteins (see Figure 3C for the domain structure of p85α). This repression can also be relieved by mutations in p110α or p85α [41]. For p85α (gene = *PIK3R1*), such mutations cluster in the iSH2 domain, and are often nonsense or frameshift mutations that result in the expression of a shortened version designated p65α [42-44]. In order to determine if the WW domain of IQGAP1 could bind to the mutationally activated p110α/p65α heterodimer, we co-translated p110α with a truncated derivative of *PIK3R1* encoding p65α (residues 1-571, Figure 3C); p110α translated alone and p65α translated alone were also included for comparison. As shown in Figure 2D, p65α alone did not display detectable binding to GST-WW, whereas p110α once again bound efficiently. However, similar to the results obtained with p85α, p65α co-translated with p110α bound to GST-WW, with an approximately 1:1 molar ratio of p65α to p110α in the bound fraction (Figure 3D, see also Supplementary Figure 1).

To summarize, the WW domain of IQGAP1 was able to bind to both the unactivated p110α/p85α heterodimer and the mutationally activated p110α/p65α heterodimer.

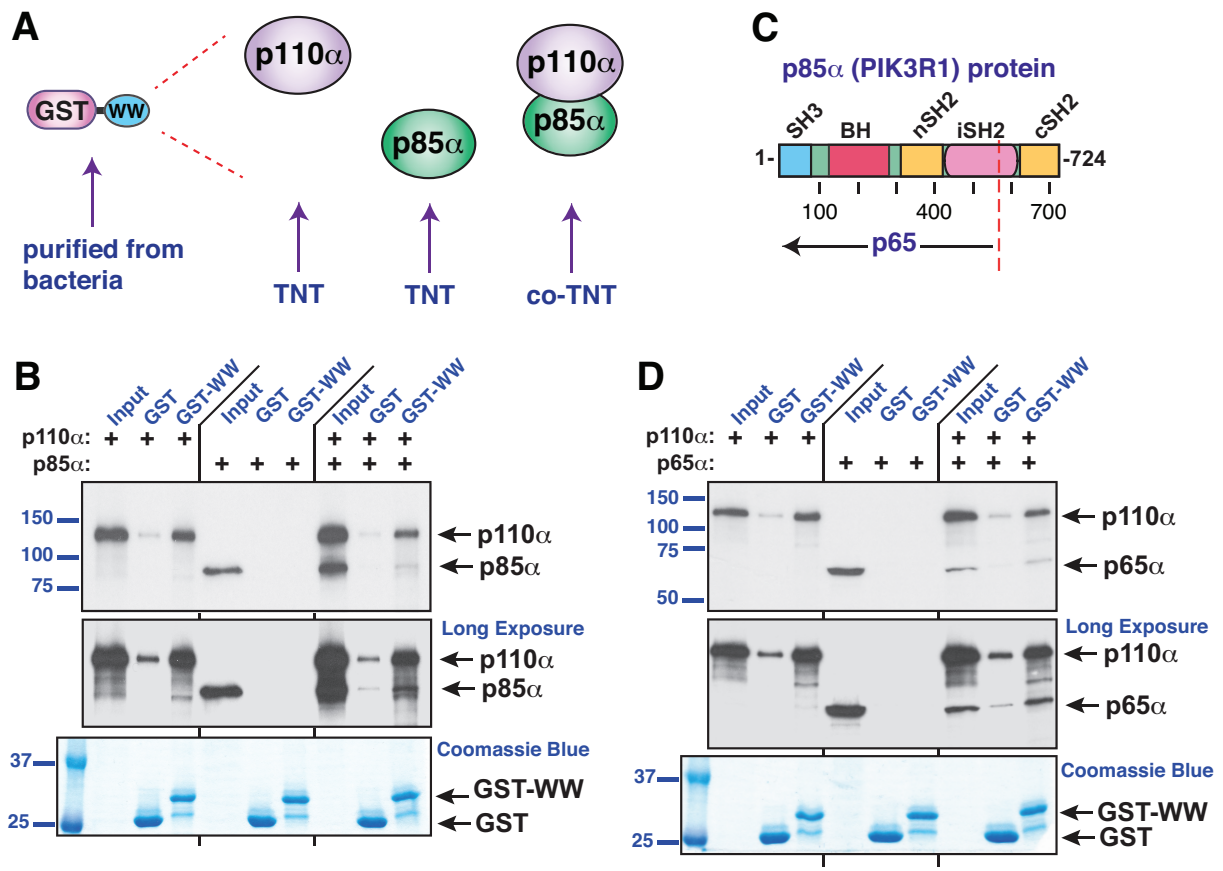

Figure 3. The WW domain of IQGAP binds to the PI 3-kinase holoenzyme.
(**A**) Human p110α and human p85α were produced by coupled *in vitro*-transcription and translation (TNT) either separately or in the same reaction ("co-TNT"), and then tested for binding to GST or GST-WW.
(**B**) Autoradiogram of a representative experiment of binding assays described in **A**. Top panel, standard exposure; middle panel, longer exposure; bottom panel, Coomassie-blue-based staining to visualize GST and GST-WW. Each binding assay shown was repeated three separate times (i.e. three independent experiments), with duplicate points (i.e. technical replicates) in each experiment. Other details as in Figure 1. After adjusting for labeling efficiency, the proportion of sedimented p85α/p110α was 1.47±0.87 (mean±95% confidence interval, n = 7); the 95% confidence interval thus includes the expected ratio of 1.0.
(**C**) Schematic depicting full-length human p85α protein with domains denoted as follows: SH3, Src-homology 3 domain; BH, BcR homology domain; nSH2, N-terminal SH2 domain; iSH2, coiled coil region between the two SH2 domains; cSH2, C-terminal SH2 domain. The position of the truncation mutation that creates the activated p65α is shown by a dashed red line.
(**D**) Human p110α and human p65α were produced by coupled *in vitro*-transcription and translation (TNT) either separately or in the same reaction, and then tested for binding to GST or GST-WW. Other details as in **B**. After adjusting for labeling efficiency, the proportion of sedimented p65α/p110α was 1.28±0.24 (mean±95% confidence interval, n = 8); the 95% confidence interval thus includes the expected ratio of 1.0.

A model of IQGAP1's WW domain

WW domains are found in plants, fungi, protists, and animals. An alignment of the WW domain of IQGAP1 with 93 other well-recognized human WW domains, a tree, sequence logos, and other analyses are presented in Supplementary Figures 2-5. These analyses revealed that the WW domains closest in sequence space to IQGAP1 include the single WW domains from IQGAP3, IQGAP2 and WAC, as well as both of the tandem WW domains from WBP4 (a.k.a. FBP21), PRPF40A (a.k.a. FBP11), PRPF40B, TCERG1 (a.k.a. FBP28) and ARHGAP12. There are no published or unpublished structures of the WW domain from any IQGAP ortholog in the Protein Data Bank. Nevertheless, by comparing the sequence of IQGAP1's WW domain to published structures of WW domains from WBP4, TCERG1 and PRPF40A [45-49], we constructed a schematic model of IQGAP1's WW domain (Figure 4A). Human IQGAP has 21 residues between the two domain-defining tryptophans, a feature shared with over 80% of human WW domains. Thus, henceforth, we will use the numbering scheme shown in Fig 4A, in which these tryptophans are at positions 1 and 23, to discuss general sequence features of WW domains. A tryptophan at position 1 and a tryptophan or phenylalanine at position 23 are found in over 95% of human WW domains, including IQGAP1's. Other sequence features that IQGAP1 shares with the majority of human WW domains include a glycine at position 9, aromatic residues at positions 12 and 13, an asparagine or aspartate at position 15, a threonine position 18, and a proline at position 26.

The schematic representation (Figure 4A) is consistent with the structure predicted by Alphafold [50, 51], which became available subsequently (Figures 4B and 4C). In this structure, the WW domain of IQGAP1 is predicted to fold into a canonical WW domain structure: an antiparallel beta sheet with three short strands connected by two loops, with main-chain hydrogen bonds providing stability (Figure 4B). As in other WW domains [46, 47, 49, 52], the side chain of the first domain-defining tryptophan (residue 1 in Figure 4A, W685 in IQGAP1) faces the underside of the sheet, where, together with the tyrosine at position 13 (Y697 in IQGAP1), the asparagine at position 15 (N699 in IQGAP1) and the proline at position 26 (P710 in IQGAP1), it constitutes a hydrophobic core that provides additional stability to the domain (Figure 4C) . Alternating side chains in the beta strands (residues 2, 4, 10, 12, 14, 16, 18, 21 and 23) face up relative to the plane of the sheet to form the top side of domain; these residues, as well as residues in one or both of the connecting loops, are frequently observed to participate in ligand binding in other WW domains [47-49, 53-56]. Collectively, these features suggest that the WW domain of IQGAP1 adopts a canonical WW domain structure [23-25]. There are, however, several differences between IQGAP1 and the consensus WW domain sequence that may be important (see further below and Discussion).

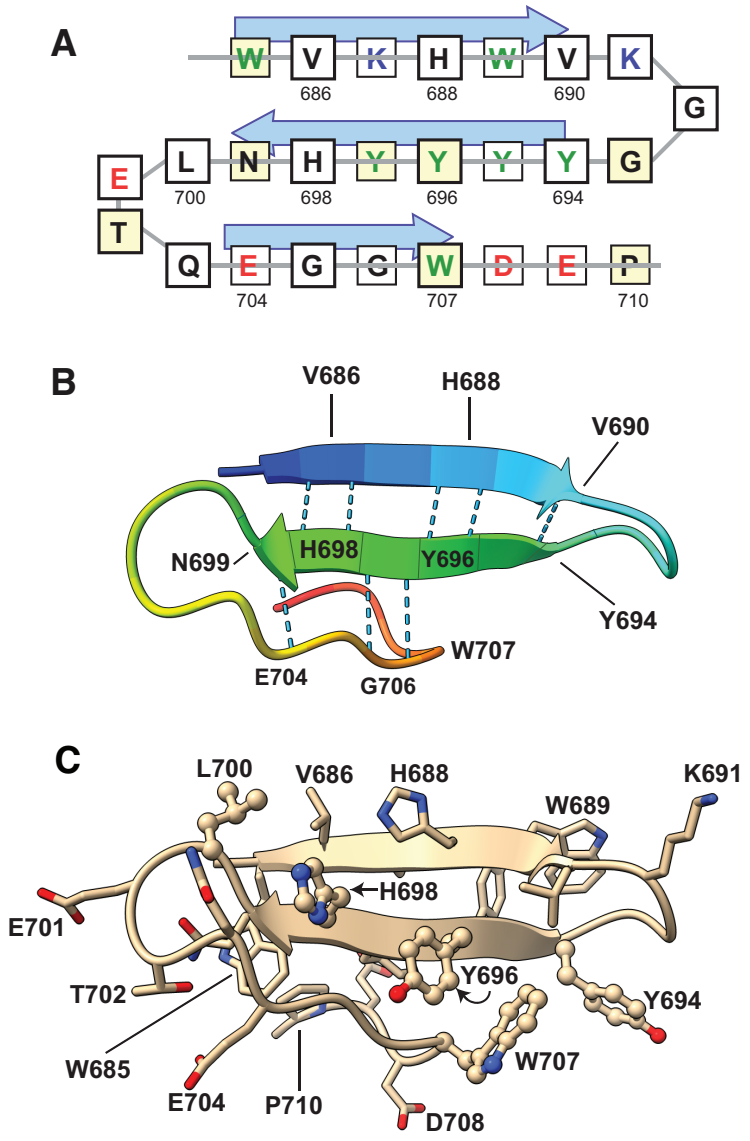

Figure 4. Model of the WW domain of human IQGAP1.
(**A**) Schematic model. Gray lines show the chain tracing, amino acid residues are shown boxed in the single-letter code. Aromatic residues (W, Y, F) are green; positively-charged residues (R, K) are blue; negatively-charged residues (D, E) are red. Residues predicted to point up are above the gray line and have slightly larger boxes with thicker outlines. Yellow boxes indicate IQGAP1 residues that are conserved in most other WW domains. Numbers below the boxes are the residue number in the 1657-residue IQGAP1 protein. Arrows show the predicted β-strands.
(**B**) Ribbon diagram derived from the Alphafold-predicted structure, colored using the rainbow coloring option of the ChimeraX software package. Main-chain hydrogen bonds between adjacent β-strand residues are shown as dotted lines; other hydrogen bonds involving side chains are not shown.
(**C**) Ribbon diagram derived from Alphafold-predicted structure with side chains shown. Side chain oxygen atoms are red, side chain nitrogen atoms are blue. The five residues subjected to single-site mutational analysis in the experiments shown in Figure 5 are shown in ball and stick format.

Conserved hydrophobic core residues in the WW domain are necessary for p110α binding

Previously, we constructed a mutant version of IQGAP1 that contained five different substitution mutations in highly conserved residues in its WW domain [32]. These 5 changes include (i) alanine substitutions to four residues that constitute a hydrophobic core on the underside of the beta sheet in other WW domains [46, 47, 49, 52], and in the predicted structure shown in Figure 4; (ii) A tyrosine-to-arginine change in a residue (position 12/Y696 in Figure 5A) whose side chain points up into the ligand binding site and helps form the proline-binding groove in other WW domains [23, 47, 49]. In our previous work, we demonstrated that these 5 mutations did not influence the binding affinity of IQGAP1 for ERK2, consistent with our finding that the IQ domain of IQGAP1 was necessary and sufficient for binding to ERK2 [32]. Here, we reintroduced those 5 mutations (W685A, Y696R, Y697A, N699A, P710A) into GST-WW and renamed this variant 'ARAAA' (see Figure 4A). We also constructed a second quintuple mutation variant of GST-WW designated 'AARAA'. This variant contains three of the above changes, plus two more substitutions to residues in the second beta strand. As shown in Figure 5B (top panels), both of these variants were completely defective for binding to p110α. The results of eight independent experiments with these two mutants is quantified in Fig. 5C, and indicated that the lack of binding exhibited by these two variants is very highly significant. Hence, combining multiple substitutions in conserved residues in the WW-domain of IQGAP1 abolished its ability to bind to p110α.

Key conserved residues in the WW domain are necessary for p110α binding

To begin to explore residues in IQGAP1's WW domain that may directly contact p110α, we used site-directed mutagenesis to examine the role of five individual residues thought to participate in ligand binding in other WW domains [45-49, 53-61]; these residues are represented in ball-and-stick format in Figure 4C. Moving from N-terminal to the C-terminal, the first residue we examined was position 10/Y694. This position, which sits at the beginning of beta strand 2, is an aromatic residue in only 4 other human WW domains; instead, most human WW domains have an arginine or lysine at this position. As shown in Figure 5B and 5C, substitution of Y694 with alanine reduced the binding of GST-WW binding to p110α by approximately 40%, and substitution with arginine abolished binding.

The next residue we examined is position 12/Y696. This residue is a tyrosine or phenylalanine in 96% of human WW domains, and its mutation to alanine [60] or arginine [58] greatly reduced ligand binding in other WW domains tested. In published structures, it is typically observed to help form the binding groove for one or more prolines in the ligand [23, 47, 49]. Interestingly, mutation of this residue to alanine had no detectable effect on GST-WW binding to p110α, nor did the more drastic substitution of arginine for the native tyrosine (Figure 5B, 5C).

In most human WW domains, the position 14 residue is usually either a branched-chain hydrophobic residue (valine, leucine or isoleucine; 63% of human WW domains) or an aromatic residue (30%). In human IQGAP1, position 14 is a histidine. Position 14 has been shown to be involved in ligand binding in multiple WW domains [47, 49, 53-55], although in none of these examples was the position 14 residue a histidine. As shown in

Figure 5C, in the IQGAP1 WW domain, a histidine to arginine substitution at position 14/H698 reduced binding by roughly 50%. Interestingly, substitution of this residue with alanine reproducibly increased binding to p110α, by an average of 250% (Figure 5D).

Position 16 has also been shown to be involved in ligand binding in multiple studies [53-56], although in all these studies the position 16 residue was a histidine, as it is in the majority (57%) of human WW domains. In human IQGAP1, position 16/L700 is a leucine. As shown in Figure 5C, substitution of L700 with either alanine or arginine both reduced binding to p110α by about 50%.

Finally**,** position 23/W707, like position 12/Y696, is typically observed to help comprise the proline-binding groove [23, 47, 49, 53]. A tryptophan to alanine substitution at this position in GST-WW reduced binding to p110α by roughly 75% (Figure 4C).

To summarize, mutational changes to four of the five individual residues we examined resulted in decreased binding to p110α, consistent with expectations based on studies of other WW domains. On the other hand, there were some possibly important differences and nuances; see Discussion for further analysis.

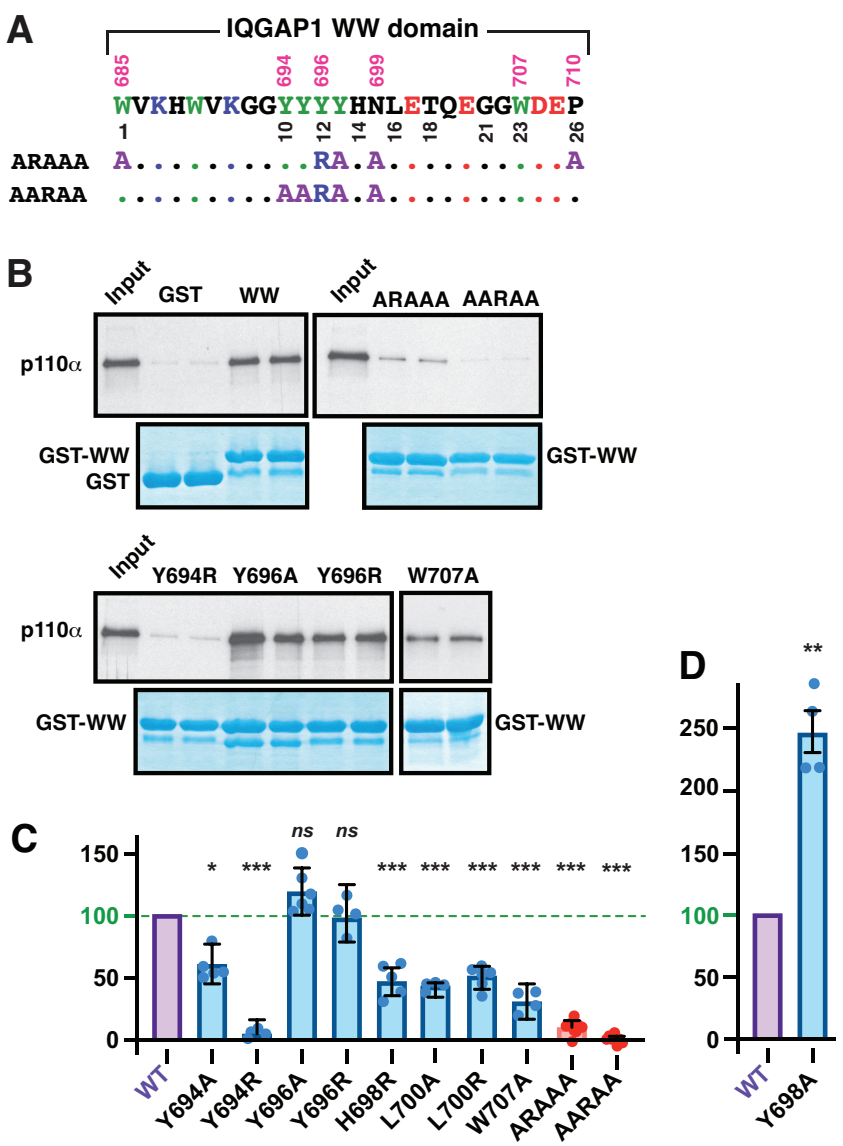

Figure 5. Structure/function analysis of the IQGAP1 WW domain by site-directed mutagenesis. (**A**) The top line shows the sequence of the WW domain of human IQGAP1. Residue numbers are shown above; the numbers below are a relative numbering system wherein the first domain-defining tryptophan of the WW domain is designated number 1. Below that, the sequence changes in two quintuplely-mutated IQGAP1 WW domain variants used in this study are shown.
(**B**) The binding of GST, GST-WW and GST-WW variants to radiolabeled p110α was assessed. Autoradiograms of representative experiments of select variants are shown.
(**C, D**) Quantification binding of GST, GST-WW and GST-WW variants to radiolabeled p110α, normalized to the percent binding of wild-type GST-WW. The results shown are the average of 4-8 independent repetitions, with duplicate points (i.e. technical replicates) in each repetition. Error bars are show the 95% confidence interval (n = 4-8). The scatter of the individual data points is also shown. Significance estimates are based on the 95% confidence interval; see Experimental Procedures for details. *ns*, not significantly differ from 100%; *, significant; **, highly significant; ***, very highly significant.

Discussion

IQGAP is a multifunctional scaffold protein that has been implicated in many physiological processes. It has an evolutionarily ancient role in regulating cytoskeletal rearrangements in fungi and animals [62, 63]. In mammals, it also functions as a scaffold protein for the RTK/RAS/MAPK pathway and the PI3K pathway – two of the pathways most frequently mutated in cancer [64-66] – and additionally regulates several other cancer-relevant signaling pathways [17-21]. Much work still needs to be done to understand how IQGAP1 and other scaffold proteins coordinate signaling in localized subcellular regions depending on cell type and cell context, how this may go awry in disease, and how it might be exploited for new targeted therapies. Despite the challenges, continued progress in this area may open new opportunities for personalized medicine. A promising direction in this regard is blocking kinase-scaffold interactions as therapeutic strategy for treating cancer and other diseases.

Here we searched for a binding partner for the WW domain of IQGAP1, motivated by recent findings that a cell-penetrating version of this domain has potent anti-tumor properties with minimal toxicity to non-transformed cells and tissues (see Introduction for further details). We found that this domain binds directly to p110α, the catalytic subunit of PI 3-kinase, which is one of the most frequently mutated proteins in human cancer. In contrast, this WW domain did not bind to ERK1, ERK2, MEK1, MEK2, or other parts of IQGAP1 (Figure1, Figure 2). Further, we found that the WW domain of IQGAP1 did not bind directly to p85α, the regulatory subunit of PI 3-kinase, but could bind to the p85α/p110α holoenzyme, in both unactivated and mutationally activated states (Figure 3).

No x-ray or NMR structures of IQGAP1's WW domain have been published. Nevertheless, by comparison to published structures of WW domains that are close in sequence to IQGAP1, we built a model of IQGAP's WW domain (Figure 4). Using this model as a reference, we then tested the role of selected residues in this WW domain on p110α binding. First, we made multiple substitutions to residues that constitute the hydrophobic core on the underside of the domain, and have been shown in other WW domains to contribute to folding and stability. Consistent with expectations, both multi-substituted variants we tested were severely defective in binding to p110α (Figure 5).

Next we tested the role of individual residues in IQGAP1's WW domain that are predicted to be situated on the ligand binding surface (Figure 5). We found that mutations to residues in positions 10, 14, 16 and 23 (see Figure 5A for numbering) all affected the binding of GST-WW to p110α. These results are consistent with the hypothesis that these residues either directly contact p110α, or influence the positioning of residues that do.

The results of mutating position 16 (L700 in IQGAP1) and position 23/W707 were the most straightforward. All tested mutations of these residues reduced binding to p110α by 50% or more. Moreover, there is considerable precedent for a direct role in ligand binding for residues in these positions in other WW domains [23, 47, 49, 53-56].

The results with position 14/H698 were more complicated, in that substitution with alanine actually increased binding to p110α by about 250%, whereas substitution with arginine reduced binding by over 50%. Interestingly, position 14 is known to be a key

residue in determining the specificity of binding in other WW domains [54]. Moreover, substitutions to the position 14 residue in the WW domain of PIN1 have also been shown to increase ligand binding affinity [67]. Modifications of H698 may thus be worth pursuing as a means to develop IQGAP1 WW peptides and peptidomimetics that have higher affinity for p110α, and therefor might perhaps display greater anti-tumor potency as well.

In many published structures of WW-ligand complexes, the position 10 residue is not observed to make direct contact with the ligand. In both cases where the position 10 residue does contact the ligand, position 10 is an arginine [59, 61]; indeed, the position 10 residue is a basic, positively charged arginine or lysine in most human WW domains. In contrast, position 10 in IQGAP1 is a tyrosine. We found that substituting this residue with arginine (Y694R) virtually eliminated binding to p110α, and that substitution with alanine reduced binding by about 40% (Figure 5). The simplest interpretation of these data is that Y694 participates directly in binding to p110α.

In most published structures of WW-ligand complexes, the position 12 residue is aromatic, as it is in IQGAP1, and is observed to make direct contact with a proline in the ligand [23, 47, 49]. Furthermore, mutation of this residue to alanine [60] or arginine [58] was found to substantially compromise binding in other WW domains tested. For IQGAP1's WW domain, however, we found that substituting this residue with either alanine (Y696A) or arginine (Y696R) had no discernable effect on binding to p110α (Figure 5). The simplest interpretation of these data is that the side chain of Y696 does not make critical contacts with p110α. Collectively, the results with position 10/Y694 and position 12/Y696 suggest that there may be some differences between how the WW domain of IQGAP1 binds p110α and the precedent established by the majority of WW domain studies. Another feature which suggests that there may be unique aspects to the manner in which the WW domain of IQGAP1 binds its ligand(s) is the presence of a glycine at position 21. IQGAP3 is the only other human WW domain containing a glycine at this position; instead, 86% of human WW domains have a serine or threonine here, and these side chains have been shown to participate in ligand binding in many instances [47, 49, 55, 56].

WW domains are proline recognition domains that typically bind to proline-rich short linear motifs in their binding partners [26]. Further work will be required to map the binding site(s) on p110α that bind to the WW domain of IQGAP1. In a systematic study of 42 WW domains that focused on identifying ligands, the WW domain of IQGAP1 was found to be unfolded under the conditions studied, and a ligand could not be identified [57]. The lack of ligand identification in this previous study cannot be solely attributed to the lack of folding, since some WW domains are observed to fold in the presence of ligand [57, 68, 69].

An updated model of IQGAP1-mediated scaffolding interactions

In this study, we found no evidence that the WW domain of IQGAP1 binds directly to p85α. Anderson and colleagues, however, have shown the IQ domain of IQGAP1 binds to both the BH and cSH2 domains of p85α [22] (see Figure 3 for p85α domain organization). A plausible model accounting for these observations is that both the WW domain and the IQ domain of IQGAP1 cooperate to bind to the p110α/p85α holoenzyme, with the WW directly contacting p110α, and the IQ domain contacting p85α. This

cooperation may function to increase the affinity of IQGAP1-PI3K binding, as well as to optimally position PI3K relative to a localized pool of its substrate PIP2. Cooperative ligand binding involving a WW domain and a neighboring domain has been observed in other cases [23]. For example, the WW domain in dystrophin cannot bind its ligand without the help of the adjacent EF hand domain [55]. Furthermore, in proteins that contain more than one WW domain, two such domains can cooperate to bind their target with higher affinity and specificity [70, 71].

Figure 6 shows a model of select binding and scaffolding interactions mediated by the WW and IQ domains of IQGAP1, based on pioneering work by other groups [12, 22, 29, 72-75], and extended by the findings presented here and in our previous study [32]. First, multiple components of the RTK/RAS/MAPK cascade –including RTKs, BRAF, MEK1/2, and ERK1/2– interact with the IQ domain of IQGAP1 (Figure 6A). Second, in the PI3K pathway, IQGAP1 interacts with PI3K using both its WW and IQ domains, the former recognizing p110α and the latter recognizing p85α (Figure 6B). IQGAP1 also interacts with PIPKI, the enzyme immediately upstream of PI3K, via its IQ domain (Figure 6B) [22, 75]. Third, we posit that cell-penetrating IQGAP1 WW peptides may block the productive engagement of PI3K with IQGAP1 by directly interfering with WW-p110 binding (Figure 6C).

Summary and conclusions

Herein we showed that the p110α catalytic subunit of human phosphoinositide 3-kinase (PI3K) is a direct binding partner of the WW domain of human IQGAP1, and made progress on the structure/function characterization of this interaction. Our findings propound a refined model of IQGAP1-mediated scaffolding, and suggest that blocking the productive engagement of PI3K with IQGAP1 is a key on-target effect of anti-neoplastic IQGAP1 WW-derived peptides.

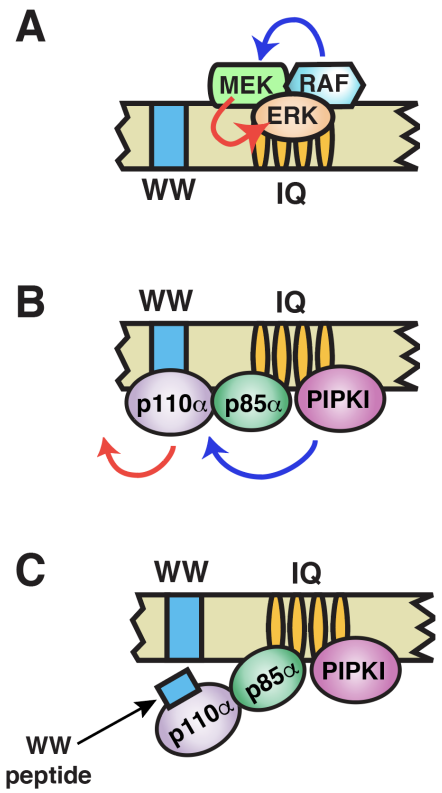

Figure 6. Model of key binding and scaffolding interactions mediated by the WW and IQ domains of IQGAP1 with elements of the MAPK and PI3K pathways.
(A) MAPK cascade interactions. Both MEK and ERK bind to the IQ domain, in close proximity to RAF and some receptor tyrosine kinases, which also bind to this domain. These interactions may facilitate RAF phosphorylation of MEK, and MEK phosphorylation of ERK. (B) PI3K pathway interactions. PI3K binds to IQGAP1 using a bipartite mechanism: p110α binds to the WW domain, and p85α binds to the IQ domain. This may position PI3K in an optimal position and orientation to utilize a localized pool of its substrate PIP2. PIP2 is generated by PIPKI, which also binds to the IQ domain. (C) We propose that cell-penetrating anti-neoplastic WW peptides may block the productive engagement of p110α with the WW domain on IQGAP1. See text for further details.

Experimental Procedures

Genes

The mammalian genes used in this study were human *IQGAP1* (NCBI accession number NM_003870), bovine *PIK3CA* (NM_174574), human *PIK3CA* (NP_006209), human *PIK3R1* (NM_181523), human *ERK1* (MAPK3; NM_002746), human *ERK2* (MAPK1, NP_620407), human *MEK1* (MAPK2K1, NM_002755), and human *MEK2* (MAP2K2, NM_030662).

IQGAP1-based constructs

GST-WW contains residues 679-719 of human IQGAP1 inserted into plasmid pGEXLB [76]. The region of interest was amplified in a polymerase chain reaction (PCR) using plasmid pCR-BluntII-TOPO-hIQGAP1 [32] as the template and primers hIQGAP1(679-x) and hIQGAP1(x-719) (See Supplementary Table 1 for all PCR primer sequences). The PCR product was cut with *BamH*I and *Sal*I and cloned into pGEXLB that had been digested with the same enzymes. For the experiment shown in Figure 4 and elsewhere, QuikChange (Agilent) was used for site-directed mutagenesis; all mutations were confirmed by sequencing.

For the experiments shown in Figure 2, the constructs for producing full-length IQGAP1 protein and IQGAP(1-678) by *in vitro* transcription/translation have been described [32]. To make IQGAP1(743-1657), the region of interest was amplified in a PCR using plasmid pCR-BluntII-TOPO-hIQGAP1 as the template and primers hIQGAP1(743-x) and hIQGAP1(x-1657). The PCR product was cut with *Xma*III and *Sal*I and cloned into pGEM3Z that had been digested with the same enzymes. The resulting construct, pGEM3Z-hIQGAP1(743-1657) contains the 743-1657 open reading frame downstream of a T7 promoter.

PIK3CA and PIK3R1-based constructs

A plasmid containing the bovine *PIK3CA* gene with an N-terminal myc-epitope tag downstream of a T7 promoter in the pCMV6 vector was obtained as a gift from TF Franke [77]. We converted this to a sequence that encodes human p110α protein by site directed mutagenesis, as the human and bovine amino acid sequences differ at only two residues. Specifically, we introduced R532K and C535S substitutions into the bovine coding sequence. The resulting plasmid is designated T7-hb-p110α, where 'hb' stands for "humanized bovine".

The C-terminal truncations p110α(1-695), p110α(1-524), p110α(1-329), p110α(1-190), and p110α(1-108) were derived by introducing stop codons at codons 696, 525, 330, 191 and 108 of the hb-p110α coding sequence via site-directed mutagenesis.

Plasmid pGEM3Z-p110α contains the coding sequence for full-length untagged human p110α protein downstream of a T7 promoter. To construct this plasmid, the human p110α-encoding open reading frame was amplified by PCR using primers p110-1-x and p110-end-down and T7-hb-p110α as the template. The resulting PCR product was digested with *BamH*I and *Sal*I and inserted into the corresponding sites of pGEM3Z.

The N-terminal deletions p110α(191-1068), p110α(330-1068), p110α(525-1068) and p110α(696-1068) were constructed by a similar PCR-based cloning procedure; see Supplementary Table 1 for primer sequences.

Plasmid pGEM3Z-p85α contains the coding sequence for full-length human p85α protein downstream of a T7 promoter. To construct this plasmid, the *PIK3R1* open reading frame was amplified by PCR using primers p85up and p85down. The template for this reaction was a human *PIK3R1* sequence-verified cDNA clone from the mammalian gene collection and sold by Dharmacon (Clone ID 30528412). The resulting PCR product was digested with *BamH*I and *Sal*I and inserted into the corresponding sites of pGEM3Z.

Plasmid pGEM3Z-p65α (encoding residues 1-571 of p85α protein) was constructed from pGEM3Z-p85α by introducing a stop codon at codon 572 of the *PIK3R1* coding sequence by site-directed mutagenesis.

In vitro transcription and translation

Proteins labeled with [^{35}S]-methionine were produced by coupled transcription and translation reactions (T7, Promega). Translation products were partially purified by ammonium sulfate precipitation [78], and resuspended in binding buffer (20mM Tris-HCl (pH 7.5), 125mM KOAc, 0.5mM EDTA, 1mM DTT, 0.1% (v/v) Tween20, 12.5% (v/v) glycerol) prior to use in binding assays.

Protein purification and binding assays

GST fusion proteins were expressed in bacteria, purified by affinity chromatography using glutathione-Sepharose (Cytiva Life Sciences) and quantified as described elsewhere [76, 79].

Protein binding assays were performed as described previously [76, 79]. Quantification of binding was performed on a Typhoon TRIO+ Imager using phosphorimaging mode. Percent binding was determined by comparing the input with the amount that was co-sedimented. This was then corrected for minor differences in loading of the GST fusion protein, which was assessed by quantifying a TIFF image of the Coomassie-blue-stained gel using ImageJ software. Each binding assay presented in this paper was repeated at least three separate times (i.e. three independent experiments), with duplicate points (i.e. technical replicates) in each experiment. Technical replicates in a given experiment are averaged together to obtain a single data point. We define 'independent experiments' as experiments performed on different days, with fresh batches of GST-fusion proteins and *in-vitro* translated proteins.

Statistical analysis

Statistical analysis of binding assay results was performed using Welch's unequal variance t-test with two tails. Where necessary, p-values were adjusted for multiple hypothesis testing using Dunnett's T3 multiple comparison test. The Graphpad Prism software package was used for statistical analysis.

For the experiment shown in Figure 5, background binding to GST was subtracted from each value, and then all measurements in that experiment were normalized by defining the binding of wild-type GST-WW to p110α as 100. This procedure complicates statistical analysis as the wild-type control (i.e. wild-type GST-WW binding to p110α) has a mean of 100 and a standard deviation of zero. Hence, we assessed significance based upon the distance between the mutant variant mean and the normalized value of 100, measured in units of the 95% confidence interval (CI) of the mean of the variant. We considered a distance of less than 1 CI as not significant ('ns' in Figure 5), a distance

between 1 and 2 CI as significant (* in Figure 5), a distance between 2 and 3 CI as highly significant (** in Figure 5), and a distance greater than 3 CI as very highly significant (*** in Figure 5).

Structural analysis

The predicted structure for human IQGAP1 is entry AF-P46940-F1 in the Alphafold database https://alphafold.ebi.ac.uk. Molecular graphics and analyses were performed with UCSF ChimeraX [80], developed by the Resource for Biocomputing, Visualization, and Informatics at the University of California, San Francisco, with support from National Institutes of Health R01-GM129325 and the Office of Cyber Infrastructure and Computational Biology, National Institute of Allergy and Infectious Diseases.

Funding

This work was supported by (1) the National Cancer Institute of the National Institutes of Health under award number P30CA062203, and the UC Irvine Comprehensive Cancer Center using UCI Anti-Cancer Challenge funds; (2) the National Center for Research Resources and the National Center for Advancing Translational Sciences, National Institutes of Health, through Grant UL1 TR001414; (3) University of California Cancer Research Coordinating Committee award CTR-20-637218.

The content of this paper is solely the responsibility of the authors and does not necessarily represent the official views of the funding agencies.

Author Contributions (CRediT format)

AJ Bardwell: conceptualization, formal analysis, investigation, methodology, supervision, validation, visualization, writing.

MD Andrade-Ludeña: investigation.

KC Yoneda: investigation.

OT Nguyen: investigation.

DA Fruman: conceptualization, formal analysis, resources.

L Bardwell: conceptualization, formal analysis, funding acquisition, investigation, methodology, project administration, supervision, validation, visualization, writing.

Conflict of Interest Statement

The authors declare that they have no conflict of interest.

References

1 Wang, X., Ni, D., Liu, Y. and Lu, S. (2021) Rational Design of Peptide-Based Inhibitors Disrupting Protein-Protein Interactions. Front Chem. **9**, 682675
2 Mullard, A. (2020) p53 programmes plough on. Nat Rev Drug Discov. **19**, 497-500
3 Schapira, M., Calabrese, M. F., Bullock, A. N. and Crews, C. M. (2019) Targeted protein degradation: expanding the toolbox. Nat Rev Drug Discov. **18**, 949-963
4 Bruzzoni-Giovanelli, H., Alezra, V., Wolff, N., Dong, C. Z., Tuffery, P. and Rebollo, A. (2018) Interfering peptides targeting protein-protein interactions: the next generation of drugs? Drug Discov Today. **23**, 272-285
5 Ashkenazi, A., Fairbrother, W. J., Leverson, J. D. and Souers, A. J. (2017) From basic apoptosis discoveries to advanced selective BCL-2 family inhibitors. Nat Rev Drug Discov. **16**, 273-284
6 Cunningham, A. D., Qvit, N. and Mochly-Rosen, D. (2017) Peptides and peptidomimetics as regulators of protein-protein interactions. Curr Opin Struct Biol. **44**, 59-66
7 Jiang, H., Deng, R., Yang, X., Shang, J., Lu, S., Zhao, Y., Song, K., Liu, X., Zhang, Q., Chen, Y., Chinn, Y. E., Wu, G., Li, J., Chen, G., Yu, J. and Zhang, J. (2017) Peptidomimetic inhibitors of APC-Asef interaction block colorectal cancer migration. Nat Chem Biol. **13**, 994-1001
8 Scott, D. E., Bayly, A. R., Abell, C. and Skidmore, J. (2016) Small molecules, big targets: drug discovery faces the protein-protein interaction challenge. Nat Rev Drug Discov. **15**, 533-550
9 Arkin, M. R., Tang, Y. and Wells, J. A. (2014) Small-molecule inhibitors of protein-protein interactions: progressing toward the reality. Chem Biol. **21**, 1102-1114
10 Chang, Y. S., Graves, B., Guerlavais, V., Tovar, C., Packman, K., To, K. H., Olson, K. A., Kesavan, K., Gangurde, P., Mukherjee, A., Baker, T., Darlak, K., Elkin, C., Filipovic, Z., Qureshi, F. Z., Cai, H., Berry, P., Feyfant, E., Shi, X. E., Horstick, J., Annis, D. A., Manning, A. M., Fotouhi, N., Nash, H., Vassilev, L. T. and Sawyer, T. K. (2013) Stapled alpha-helical peptide drug development: a potent dual inhibitor of MDM2 and MDMX for p53-dependent cancer therapy. Proc Natl Acad Sci U S A. **110**, E3445-3454
11 Souers, A. J., Leverson, J. D., Boghaert, E. R., Ackler, S. L., Catron, N. D., Chen, J., Dayton, B. D., Ding, H., Enschede, S. H., Fairbrother, W. J., Huang, D. C., Hymowitz, S. G., Jin, S., Khaw, S. L., Kovar, P. J., Lam, L. T., Lee, J., Maecker, H. L., Marsh, K. C., Mason, K. D., Mitten, M. J., Nimmer, P. M., Oleksijew, A., Park, C. H., Park, C. M., Phillips, D. C., Roberts, A. W., Sampath, D., Seymour, J. F., Smith, M. L., Sullivan, G. M., Tahir, S. K., Tse, C., Wendt, M. D., Xiao, Y., Xue, J. C., Zhang, H., Humerickhouse, R. A., Rosenberg, S. H. and Elmore, S. W. (2013) ABT-199, a potent and selective BCL-2 inhibitor, achieves antitumor activity while sparing platelets. Nat Med. **19**, 202-208
12 Jameson, K. L., Mazur, P. K., Zehnder, A. M., Zhang, J., Zarnegar, B., Sage, J. and Khavari, P. A. (2013) IQGAP1 scaffold-kinase interaction blockade selectively targets RAS-MAP kinase-driven tumors. Nat Med. **19**, 626-630
13 Sanchez-Laorden, B., Viros, A. and Marais, R. (2013) Mind the IQGAP. Cancer Cell. **23**, 715-717

14 Stuart, D. D. and Sellers, W. R. (2013) Targeting RAF-MEK-ERK kinase-scaffold interactions in cancer. Nat Med. **19**, 538-540
15 Schambach, A., Schott, J. W. and Morgan, M. A. (2017) Uncoupling the Oncogenic Engine. Cancer Res. **77**, 6060-6064
16 Pudewell, S., Wittich, C., Kazemein Jasemi, N. S., Bazgir, F. and Ahmadian, M. R. (2021) Accessory proteins of the RAS-MAPK pathway: moving from the side line to the front line. Commun Biol. **4**, 696
17 Wei, T. and Lambert, P. F. (2021) Role of IQGAP1 in Carcinogenesis. Cancers (Basel). **13**
18 Peng, X., Wang, T., Gao, H., Yue, X., Bian, W., Mei, J. and Zhang, Y. (2021) The interplay between IQGAP1 and small GTPases in cancer metastasis. Biomed Pharmacother. **135**, 111243
19 Abel, A. M., Schuldt, K. M., Rajasekaran, K., Hwang, D., Riese, M. J., Rao, S., Thakar, M. S. and Malarkannan, S. (2015) IQGAP1: insights into the function of a molecular puppeteer. Mol Immunol. **65**, 336-349
20 Hedman, A. C., Smith, J. M. and Sacks, D. B. (2015) The biology of IQGAP proteins: beyond the cytoskeleton. EMBO Rep. **16**, 427-446
21 Johnson, M., Sharma, M. and Henderson, B. R. (2009) IQGAP1 regulation and roles in cancer. Cell Signal. **21**, 1471-1478
22 Choi, S., Hedman, A. C., Sayedyahossein, S., Thapa, N., Sacks, D. B. and Anderson, R. A. (2016) Agonist-stimulated phosphatidylinositol-3,4,5-trisphosphate generation by scaffolded phosphoinositide kinases. Nat Cell Biol. **18**, 1324-1335
23 Zarrinpar, A. and Lim, W. A. (2000) Converging on proline: the mechanism of WW domain peptide recognition. Nat Struct Biol. **7**, 611-613
24 Macias, M. J., Wiesner, S. and Sudol, M. (2002) WW and SH3 domains, two different scaffolds to recognize proline-rich ligands. FEBS Lett. **513**, 30-37
25 Sudol, M., Shields, D. C. and Farooq, A. (2012) Structures of YAP protein domains reveal promising targets for development of new cancer drugs. Semin Cell Dev Biol. **23**, 827-833
26 Zarrinpar, A., Bhattacharyya, R. P. and Lim, W. A. (2003) The structure and function of proline recognition domains. Sci STKE. **2003**, RE8
27 Li, J. H., McMillan, R. H., Begum, A., Gocke, C. B. and Matsui, W. (2019) IQGAP1 Maintains Pancreatic Ductal Adenocarcinoma Clonogenic Growth and Metastasis. Pancreas. **48**, 94-98
28 Gocke, C. B., McMillan, R., Wang, Q., Begum, A., Penchev, V. R., Ali, S. A., Borrello, I., Huff, C. A. and Matsui, W. (2016) IQGAP1 Scaffold-MAP Kinase Interactions Enhance Multiple Myeloma Clonogenic Growth and Self-Renewal. Mol Cancer Ther. **15**, 2733-2739
29 Roy, M., Li, Z. and Sacks, D. B. (2005) IQGAP1 is a scaffold for mitogen-activated protein kinase signaling. Mol Cell Biol. **25**, 7940-7952
30 Roy, M., Li, Z. and Sacks, D. B. (2004) IQGAP1 binds ERK2 and modulates its activity. J Biol Chem. **279**, 17329-17337
31 White, C. D., Erdemir, H. H. and Sacks, D. B. (2012) IQGAP1 and its binding proteins control diverse biological functions. Cell Signal. **24**, 826-834

32 Bardwell, A. J., Lagunes, L., Zebarjedi, R. and Bardwell, L. (2017) The WW domain of the scaffolding protein IQGAP1 is neither necessary nor sufficient for binding to the MAPKs ERK1 and ERK2. J Biol Chem. **292**, 8750-8761
33 Fruman, D. A. and Rommel, C. (2014) PI3K and cancer: lessons, challenges and opportunities. Nat Rev Drug Discov. **13**, 140-156
34 Thorpe, L. M., Yuzugullu, H. and Zhao, J. J. (2015) PI3K in cancer: divergent roles of isoforms, modes of activation and therapeutic targeting. Nat Rev Cancer. **15**, 7-24
35 Fruman, D. A., Chiu, H., Hopkins, B. D., Bagrodia, S., Cantley, L. C. and Abraham, R. T. (2017) The PI3K Pathway in Human Disease. Cell. **170**, 605-635
36 Dornan, G. L. and Burke, J. E. (2018) Molecular Mechanisms of Human Disease Mediated by Oncogenic and Primary Immunodeficiency Mutations in Class IA Phosphoinositide 3-Kinases. Front Immunol. **9**, 575
37 Madsen, R. R., Vanhaesebroeck, B. and Semple, R. K. (2018) Cancer-Associated PIK3CA Mutations in Overgrowth Disorders. Trends Mol Med. **24**, 856-870
38 Lin, Z., Xie, R., Guan, K. and Zhang, M. (2020) A WW Tandem-Mediated Dimerization Mode of SAV1 Essential for Hippo Signaling. Cell Rep. **32**, 108118
39 Gao, Y. G., Yang, H., Zhao, J., Jiang, Y. J. and Hu, H. Y. (2014) Autoinhibitory structure of the WW domain of HYPB/SETD2 regulates its interaction with the proline-rich region of huntingtin. Structure. **22**, 378-386
40 Fox, M., Mott, H. R. and Owen, D. (2020) Class IA PI3K regulatory subunits: p110-independent roles and structures. Biochem Soc Trans. **48**, 1397-1417
41 Burke, J. E. (2018) Structural Basis for Regulation of Phosphoinositide Kinases and Their Involvement in Human Disease. Mol Cell. **71**, 653-673
42 Jimenez, C., Hernandez, C., Pimentel, B. and Carrera, A. C. (2002) The p85 regulatory subunit controls sequential activation of phosphoinositide 3-kinase by Tyr kinases and Ras. J Biol Chem. **277**, 41556-41562
43 Jaiswal, B. S., Janakiraman, V., Kljavin, N. M., Chaudhuri, S., Stern, H. M., Wang, W., Kan, Z., Dbouk, H. A., Peters, B. A., Waring, P., Dela Vega, T., Kenski, D. M., Bowman, K. K., Lorenzo, M., Li, H., Wu, J., Modrusan, Z., Stinson, J., Eby, M., Yue, P., Kaminker, J. S., de Sauvage, F. J., Backer, J. M. and Seshagiri, S. (2009) Somatic mutations in p85alpha promote tumorigenesis through class IA PI3K activation. Cancer Cell. **16**, 463-474
44 Cheung, L. W. and Mills, G. B. (2016) Targeting therapeutic liabilities engendered by PIK3R1 mutations for cancer treatment. Pharmacogenomics. **17**, 297-307
45 Macias, M. J., Gervais, V., Civera, C. and Oschkinat, H. (2000) Structural analysis of WW domains and design of a WW prototype. Nat Struct Biol. **7**, 375-379
46 Pires, J. R., Parthier, C., Aido-Machado, R., Wiedemann, U., Otte, L., Bohm, G., Rudolph, R. and Oschkinat, H. (2005) Structural basis for APPTPPPLPP peptide recognition by the FBP11WW1 domain. J Mol Biol. **348**, 399-408
47 Kato, Y., Hino, Y., Nagata, K. and Tanokura, M. (2006) Solution structure and binding specificity of FBP11/HYPA WW domain as Group-II/III. Proteins. **63**, 227-234
48 Ramirez-Espain, X., Ruiz, L., Martin-Malpartida, P., Oschkinat, H. and Macias, M. J. (2007) Structural characterization of a new binding motif and a novel binding mode in group 2 WW domains. J Mol Biol. **373**, 1255-1268

49 Huang, X., Beullens, M., Zhang, J., Zhou, Y., Nicolaescu, E., Lesage, B., Hu, Q., Wu, J., Bollen, M. and Shi, Y. (2009) Structure and function of the two tandem WW domains of the pre-mRNA splicing factor FBP21 (formin-binding protein 21). J Biol Chem. **284**, 25375-25387
50 Varadi, M., Anyango, S., Deshpande, M., Nair, S., Natassia, C., Yordanova, G., Yuan, D., Stroe, O., Wood, G., Laydon, A., Zidek, A., Green, T., Tunyasuvunakool, K., Petersen, S., Jumper, J., Clancy, E., Green, R., Vora, A., Lutfi, M., Figurnov, M., Cowie, A., Hobbs, N., Kohli, P., Kleywegt, G., Birney, E., Hassabis, D. and Velankar, S. (2022) AlphaFold Protein Structure Database: massively expanding the structural coverage of protein-sequence space with high-accuracy models. Nucleic Acids Res. **50**, D439-D444
51 Jumper, J., Evans, R., Pritzel, A., Green, T., Figurnov, M., Ronneberger, O., Tunyasuvunakool, K., Bates, R., Zidek, A., Potapenko, A., Bridgland, A., Meyer, C., Kohl, S. A. A., Ballard, A. J., Cowie, A., Romera-Paredes, B., Nikolov, S., Jain, R., Adler, J., Back, T., Petersen, S., Reiman, D., Clancy, E., Zielinski, M., Steinegger, M., Pacholska, M., Berghammer, T., Bodenstein, S., Silver, D., Vinyals, O., Senior, A. W., Kavukcuoglu, K., Kohli, P. and Hassabis, D. (2021) Highly accurate protein structure prediction with AlphaFold. Nature. **596**, 583-589
52 Jager, M., Dendle, M. and Kelly, J. W. (2009) Sequence determinants of thermodynamic stability in a WW domain--an all-beta-sheet protein. Protein Sci. **18**, 1806-1813
53 Macias, M. J., Hyvonen, M., Baraldi, E., Schultz, J., Sudol, M., Saraste, M. and Oschkinat, H. (1996) Structure of the WW domain of a kinase-associated protein complexed with a proline-rich peptide. Nature. **382**, 646-649
54 Espanel, X. and Sudol, M. (1999) A single point mutation in a group I WW domain shifts its specificity to that of group II WW domains. J Biol Chem. **274**, 17284-17289
55 Huang, X., Poy, F., Zhang, R., Joachimiak, A., Sudol, M. and Eck, M. J. (2000) Structure of a WW domain containing fragment of dystrophin in complex with beta-dystroglycan. Nat Struct Biol. **7**, 634-638
56 Kasanov, J., Pirozzi, G., Uveges, A. J. and Kay, B. K. (2001) Characterizing Class I WW domains defines key specificity determinants and generates mutant domains with novel specificities. Chem Biol. **8**, 231-241
57 Otte, L., Wiedemann, U., Schlegel, B., Pires, J. R., Beyermann, M., Schmieder, P., Krause, G., Volkmer-Engert, R., Schneider-Mergener, J. and Oschkinat, H. (2003) WW domain sequence activity relationships identified using ligand recognition propensities of 42 WW domains. Protein Sci. **12**, 491-500
58 Aqeilan, R. I., Donati, V., Palamarchuk, A., Trapasso, F., Kaou, M., Pekarsky, Y., Sudol, M. and Croce, C. M. (2005) WW domain-containing proteins, WWOX and YAP, compete for interaction with ErbB-4 and modulate its transcriptional function. Cancer Res. **65**, 6764-6772
59 Aragon, E., Goerner, N., Xi, Q., Gomes, T., Gao, S., Massague, J. and Macias, M. J. (2012) Structural basis for the versatile interactions of Smad7 with regulator WW domains in TGF-beta Pathways. Structure. **20**, 1726-1736
60 Vargas, R. E., Duong, V. T., Han, H., Ta, A. P., Chen, Y., Zhao, S., Yang, B., Seo, G., Chuc, K., Oh, S., El Ali, A., Razorenova, O. V., Chen, J., Luo, R., Li, X. and

Wang, W. (2020) Elucidation of WW domain ligand binding specificities in the Hippo pathway reveals STXBP4 as YAP inhibitor. EMBO J. **39**, e102406
61 Rheinemann, L., Thompson, T., Mercenne, G., Paine, E. L., Peterson, F. C., Volkman, B. F., Alam, S. L., Alian, A. and Sundquist, W. I. (2021) Interactions between AMOT PPxY motifs and NEDD4L WW domains function in HIV-1 release. J Biol Chem. **297**, 100975
62 Shannon, K. B. (2012) IQGAP Family Members in Yeast, Dictyostelium, and Mammalian Cells. Int J Cell Biol. **2012**, 894817
63 Pollard, T. D. and O'Shaughnessy, B. (2019) Molecular Mechanism of Cytokinesis. Annu Rev Biochem. **88**, 661-689
64 Zhang, Y., Kwok-Shing Ng, P., Kucherlapati, M., Chen, F., Liu, Y., Tsang, Y. H., de Velasco, G., Jeong, K. J., Akbani, R., Hadjipanayis, A., Pantazi, A., Bristow, C. A., Lee, E., Mahadeshwar, H. S., Tang, J., Zhang, J., Yang, L., Seth, S., Lee, S., Ren, X., Song, X., Sun, H., Seidman, J., Luquette, L. J., Xi, R., Chin, L., Protopopov, A., Westbrook, T. F., Shelley, C. S., Choueiri, T. K., Ittmann, M., Van Waes, C., Weinstein, J. N., Liang, H., Henske, E. P., Godwin, A. K., Park, P. J., Kucherlapati, R., Scott, K. L., Mills, G. B., Kwiatkowski, D. J. and Creighton, C. J. (2017) A Pan-Cancer Proteogenomic Atlas of PI3K/AKT/mTOR Pathway Alterations. Cancer Cell. **31**, 820-832 e823
65 Sanchez-Vega, F., Mina, M., Armenia, J., Chatila, W. K., Luna, A., La, K. C., Dimitriadoy, S., Liu, D. L., Kantheti, H. S., Saghafinia, S., Chakravarty, D., Daian, F., Gao, Q., Bailey, M. H., Liang, W. W., Foltz, S. M., Shmulevich, I., Ding, L., Heins, Z., Ochoa, A., Gross, B., Gao, J., Zhang, H., Kundra, R., Kandoth, C., Bahceci, I., Dervishi, L., Dogrusoz, U., Zhou, W., Shen, H., Laird, P. W., Way, G. P., Greene, C. S., Liang, H., Xiao, Y., Wang, C., Iavarone, A., Berger, A. H., Bivona, T. G., Lazar, A. J., Hammer, G. D., Giordano, T., Kwong, L. N., McArthur, G., Huang, C., Tward, A. D., Frederick, M. J., McCormick, F., Meyerson, M., Cancer Genome Atlas Research, N., Van Allen, E. M., Cherniack, A. D., Ciriello, G., Sander, C. and Schultz, N. (2018) Oncogenic Signaling Pathways in The Cancer Genome Atlas. Cell. **173**, 321-337 e310
66 Bailey, M. H., Tokheim, C., Porta-Pardo, E., Sengupta, S., Bertrand, D., Weerasinghe, A., Colaprico, A., Wendl, M. C., Kim, J., Reardon, B., Ng, P. K., Jeong, K. J., Cao, S., Wang, Z., Gao, J., Gao, Q., Wang, F., Liu, E. M., Mularoni, L., Rubio-Perez, C., Nagarajan, N., Cortes-Ciriano, I., Zhou, D. C., Liang, W. W., Hess, J. M., Yellapantula, V. D., Tamborero, D., Gonzalez-Perez, A., Suphavilai, C., Ko, J. Y., Khurana, E., Park, P. J., Van Allen, E. M., Liang, H., Group, M. C. W., Cancer Genome Atlas Research, N., Lawrence, M. S., Godzik, A., Lopez-Bigas, N., Stuart, J., Wheeler, D., Getz, G., Chen, K., Lazar, A. J., Mills, G. B., Karchin, R. and Ding, L. (2018) Comprehensive Characterization of Cancer Driver Genes and Mutations. Cell. **173**, 371-385 e318
67 Verdecia, M. A., Bowman, M. E., Lu, K. P., Hunter, T. and Noel, J. P. (2000) Structural basis for phosphoserine-proline recognition by group IV WW domains. Nat Struct Biol. **7**, 639-643
68 Ji, Z., Li, H., Yang, Z., Huang, X., Ke, X., Ma, S., Lin, Z., Lu, Y. and Zhang, M. (2019) Kibra Modulates Learning and Memory via Binding to Dendrin. Cell Rep. **26**, 2064-2077 e2067

69 Panwalkar, V., Neudecker, P., Schmitz, M., Lecher, J., Schulte, M., Medini, K., Stoldt, M., Brimble, M. A., Willbold, D. and Dingley, A. J. (2016) The Nedd4-1 WW Domain Recognizes the PY Motif Peptide through Coupled Folding and Binding Equilibria. Biochemistry. **55**, 659-674
70 Lin, Z., Yang, Z., Xie, R., Ji, Z., Guan, K. and Zhang, M. (2019) Decoding WW domain tandem-mediated target recognitions in tissue growth and cell polarity. Elife. **8**
71 Dodson, E. J., Fishbain-Yoskovitz, V., Rotem-Bamberger, S. and Schueler-Furman, O. (2015) Versatile communication strategies among tandem WW domain repeats. Exp Biol Med (Maywood). **240**, 351-360
72 Ren, J. G., Li, Z. and Sacks, D. B. (2007) IQGAP1 modulates activation of B-Raf. Proc Natl Acad Sci U S A. **104**, 10465-10469
73 McNulty, D. E., Li, Z., White, C. D., Sacks, D. B. and Annan, R. S. (2011) MAPK scaffold IQGAP1 binds the EGF receptor and modulates its activation. J Biol Chem. **286**, 15010-15021
74 Chen, M., Choi, S., Jung, O., Wen, T., Baum, C., Thapa, N., Lambert, P. F., Rapraeger, A. C. and Anderson, R. A. (2019) The Specificity of EGF-Stimulated IQGAP1 Scaffold Towards the PI3K-Akt Pathway is Defined by the IQ3 motif. Sci Rep. **9**, 9126
75 Choi, S., Thapa, N., Hedman, A. C., Li, Z., Sacks, D. B. and Anderson, R. A. (2013) IQGAP1 is a novel phosphatidylinositol 4,5 bisphosphate effector in regulation of directional cell migration. EMBO J. **32**, 2617-2630
76 Bardwell, A. J., Flatauer, L. J., Matsukuma, K., Thorner, J. and Bardwell, L. (2001) A conserved docking site in MEKs mediates high-affinity binding to MAP kinases and cooperates with a scaffold protein to enhance signal transmission. J Biol Chem. **276**, 10374-10386
77 Franke, T. F., Kaplan, D. R., Cantley, L. C. and Toker, A. (1997) Direct regulation of the Akt proto-oncogene product by phosphatidylinositol-3,4-bisphosphate. Science. **275**, 665-668
78 Bardwell, L. and Shah, K. (2006) Analysis of mitogen-activated protein kinase activation and interactions with regulators and substrates. Methods. **40**, 213-223
79 Gordon, E. A., Whisenant, T. C., Zeller, M., Kaake, R. M., Gordon, W. M., Krotee, P., Patel, V., Huang, L., Baldi, P. and Bardwell, L. (2013) Combining docking site and phosphosite predictions to find new substrates: identification of smoothelin-like-2 (SMTNL2) as a c-Jun N-terminal kinase (JNK) substrate. Cell Signal. **25**, 2518-2529
80 Pettersen, E. F., Goddard, T. D., Huang, C. C., Meng, E. C., Couch, G. S., Croll, T. I., Morris, J. H. and Ferrin, T. E. (2021) UCSF ChimeraX: Structure visualization for researchers, educators, and developers. Protein Sci. **30**, 70-82
81 Crooks, G. E., Hon, G., Chandonia, J. M. and Brenner, S. E. (2004) WebLogo: a sequence logo generator. Genome Res. **14**, 1188-1190

Supplementary Figures

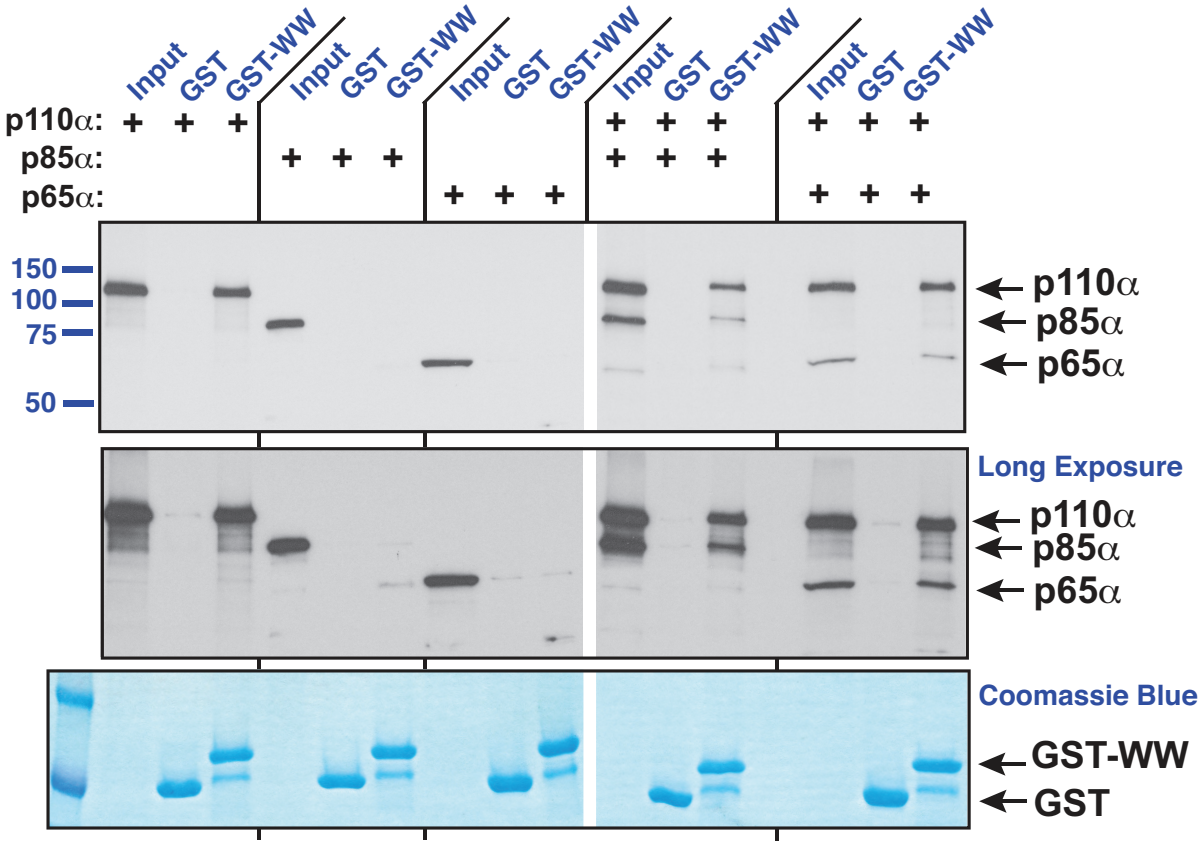

Supplementary Figure 1. The WW domain of IQGAP binds to p110α/p85α and p110α/p65α heterodimers.
Human p110α, p85α, and p65α were produced by coupled *in vitro*-transcription and translation (TNT) in separate reactions. In addition, p110α + p85α were both translated in the same reaction, and p110α + p65α were both translated in the same reaction. The products of these 5 TNT reactions were then each tested for binding to GST or GST-WW. The figure shows an autoradiogram of a representative experiment (the experiment is different from that shown in Figure 3B and 3D). Top panel, standard exposure; middle panel, longer exposure; bottom panel, Coomassie-blue-based staining to visualize GST and GST-WW. Other details as in Figure 1.

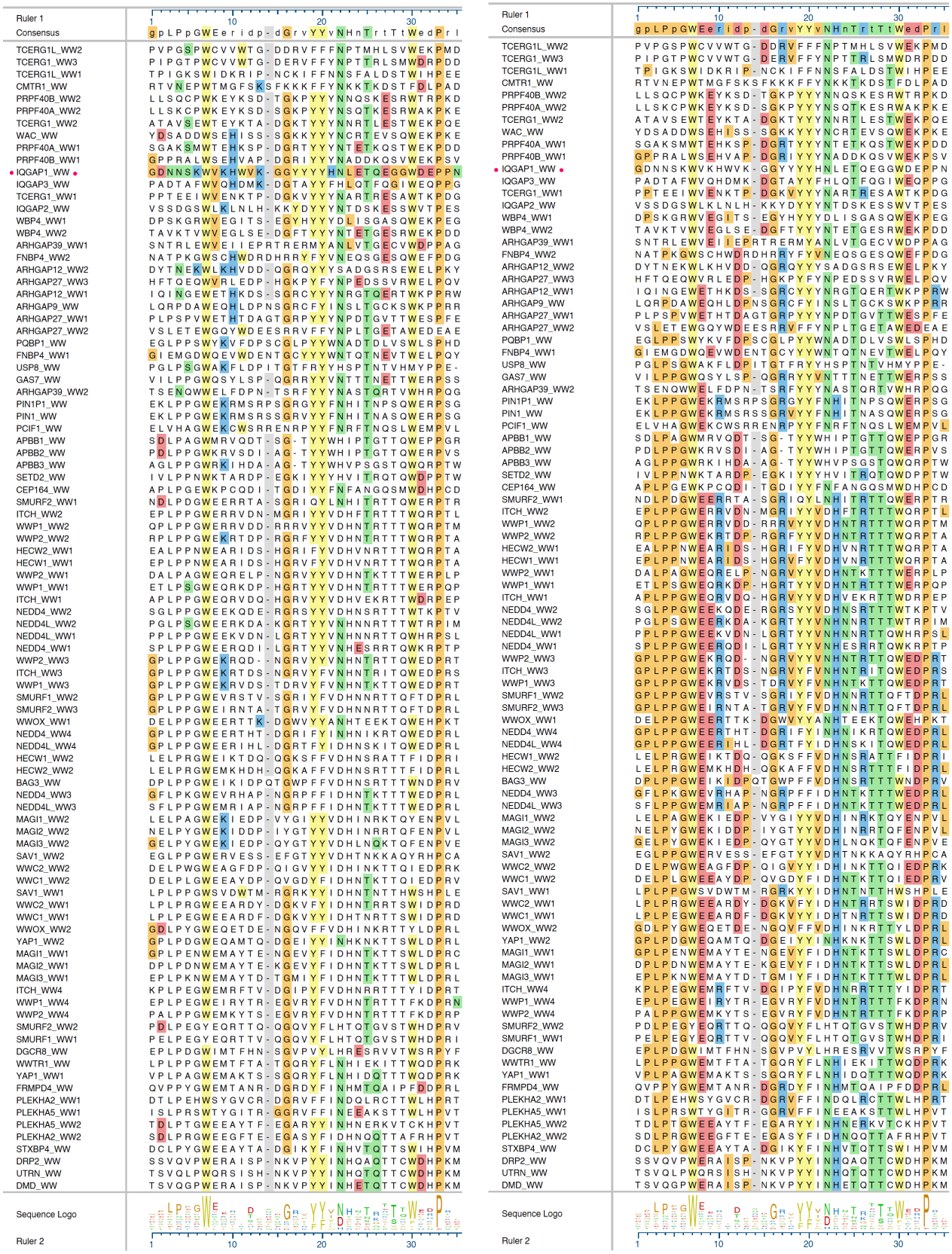

Supplementary Figure 2. Alignment of 94 human WW domains

Supplementary Figure 2. Alignment of 94 human WW domains.

The sequences are listed in the order shown in the Tree in Supplementary Figure 3. The left and right alignments are identical except for coloring. On the left, residues are colored if they match IQGAP1; On the right, residues are colored if they match the consensus shown on top. The color scheme is as follows: aromatic residues (F, Y, W) are yellow, acidic residues (D, E) are red, nonpolar residues (A, G, I, L, M, P, V) are orange, polar residues (C, N, Q, S, T) are green. The numbering on the rulers are different than the numbering Figure 5A. To convert, subtract 6 from the ruler numbers to the left of the gap in the IQGAP1 sequence and subtract 7 from the ruler numbers to the right of the gap. The alignment was generated using MegAlign Pro version 17.3.1 (DNASTAR, Inc.) using the MAFFT L-ins-I algorithm with a gap open penalty of 3 and a gap extension penalty of 0. BLOSUM62 was used as the scoring matrix.

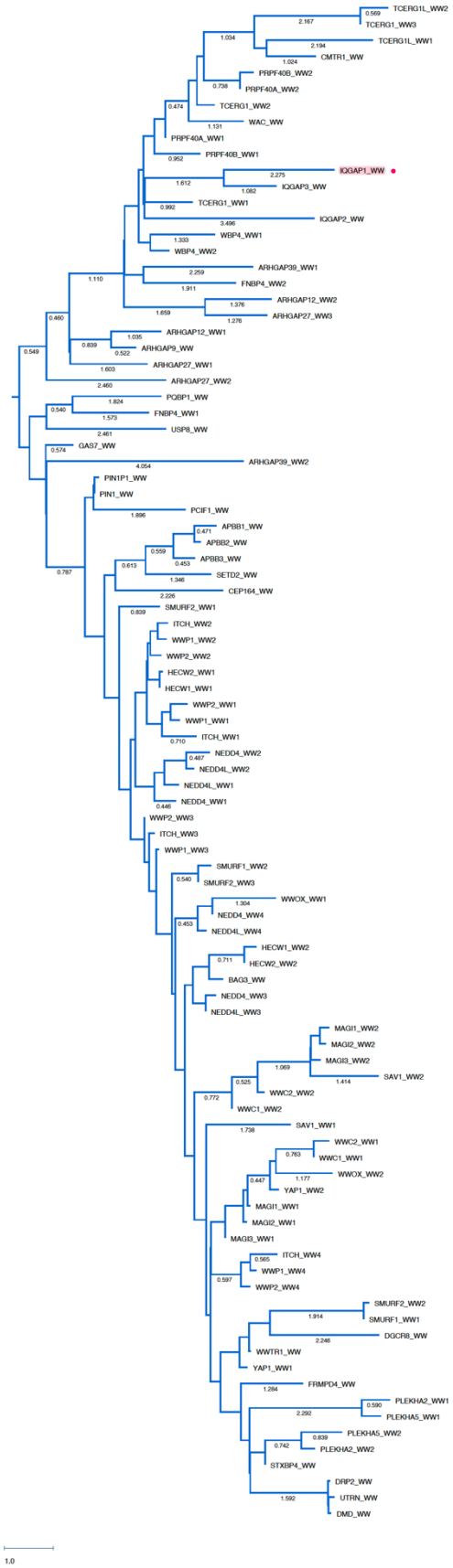

Supplementary Figure 3.
Sequence tree of 94 human WW domains.

Sequence identity tree generated from the alignment shown in Supplementary Figure 2, using the maximum likelihood method using uncorrected pairwise distance and pairwise gap removal options. Other details as in Supplementary Figure 2.

Sort by Similarity		Sort by Identity		Sort by Score	
Designation	Similarity	Designation	Identity	Designation	Score
IQGAP1_WW	100.0	IQGAP1_WW	100.0	IQGAP1_WW	213
IQGAP3_WW	64.7	IQGAP3_WW	38.2	IQGAP3_WW	77
WBP4_WW2	55.9	FNBP4_WW1	35.3	PRPF40A_WW1	68
PRPF40A_WW1	52.9	ARHGAP12_WW1	35.3	WBP4_WW2	62
IQGAP2_WW	52.9	WBP4_WW2	32.4	WAC_WW	60
WBP4_WW1	52.9	PRPF40A_WW1	32.4	WBP4_WW1	59
PRPF40B_WW1	50.0	WWP2_WW3	30.3	TCERG1_WW1	58
FNBP4_WW1	47.1	TCERG1_WW2	29.4	PRPF40B_WW1	57
TCERG1_WW2	47.1	WAC_WW	29.4	FNBP4_WW1	55
WAC_WW	47.1	ARHGAP12_WW2	29.4	TCERG1_WW2	55
PRPF40A_WW2	47.1	TCERG1_WW1	29.4	ARHGAP12_WW2	54
PRPF40B_WW2	47.1	ARHGAP39_WW1	29.4	IQGAP2_WW	53
CMTR1_WW	47.1	DMD_WW	29.4	ARHGAP12_WW1	51
ARHGAP27_WW2	47.1	IQGAP2_WW	26.5	PRPF40A_WW2	45
ARHGAP12_WW2	44.1	WBP4_WW1	26.5	WWOX_WW1	43
TCERG1_WW1	44.1	PRPF40B_WW1	26.5	ARHGAP39_WW2	42
APBB1_WW	42.4	PRPF40A_WW2	26.5	FNBP4_WW2	40
ARHGAP12_WW1	41.2	FNBP4_WW2	26.5	APBB1_WW	39
FNBP4_WW2	41.2	ITCH_WW3	26.5	ITCH_WW3	39
ITCH_WW3	41.2	PCIF1_WW	26.5	PRPF40B_WW2	39
PCIF1_WW	41.2	ARHGAP27_WW1	26.5	WWP2_WW3	36
WWOX_WW1	41.2	GAS7_WW	26.5	DMD_WW	35

Supplementary Figure 4. Human WW domains most closely related to the WW domain in human IQGAP1.

Relatedness to IQGAP1's WW domain was assessed by three methods: sequence similarity (left columns), sequence identity (middle columns), and the score generated by a Needleman-Wunsch global pairwise alignment with a gap penalty of 10, a gap extension penalty of 10, and BLOSUM62 used as the scoring matrix. The top 25 in each category are shown. Select WW domains are color coded as a visual aid. The sequences used are the same as shown in Supplementary Figure 2.

Human WW domains

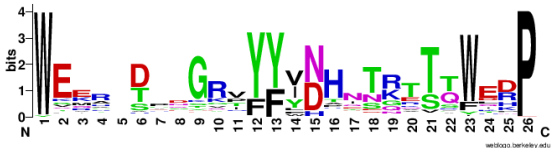

Mammalian IQGAP1:

Bird IQGAP1:

Reptile IQGAP1:

Amphibian IQGAP1:

Bony Fish IQGAP1:

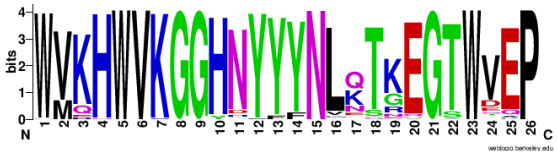

Other Fish IQGAP1:

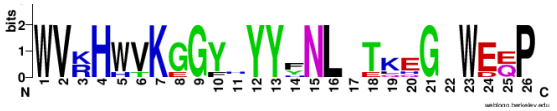

Supplementary Figure 5. Sequence logos of human WW domains and of vertebrate IQGAP1 orthologs.

The sequence logos were created with WebLogo [81]. Residue numbering as in Figure 5A. Vertebrate ortholog sequences used to create the logos are from the National Center for Biotechnology Information (NCBI) page on IQGAP1 orthologs: https://www.ncbi.nlm.nih.gov/gene/8826/ortholog/?scope=89593.

Supplementary Table 1. PCR primers used in this study.

Name	Sequence (5'→3')	Use
hIQGAP1(679-x)	ggaggcggtGGATCCacc**ATG**ggagataataacagcaagtgg	GST-WW
hIQGAP1(x-719)	gccgctcgaGTCGAC**TTA**ctgcatagaattttgcacaaaa	GST-WW
hIQGAP1(743-x)	agctcggtaCCCGGGacc**ATG**ctggccaatgaaggcctga	IQGAP1(743-1657)
hIQGAP1(x-1657)	tgcctgcagGTCGACtggcagcaaacgatcaa**TTA**	IQGAP1(743-1657)
p110-1-x	gcgGGATCCacc**ATG**cctccaagaccatcatca	p110a(1-1068)
p110-end-down	cgGTCGAC**TTA**gttcaaagcatgctgctt	p110a(x-1068)
p110-191-end-up	gcgGGATCCacc**ATG**atagtggtgatttgggta	p110a(191-1068)
p110-330-end-up	gcgGGATCCacc**ATG**ataaatagtgcactcaga	p110a(330-1068)
p110-525-end-up	gcgGGATCCacc**ATG**gaaaatgataaagaacag	p110a(525-1068)
p110-696-end-up	gcgGGATCCacc**ATG**gggatgtatctgaagcac	p110a(696-1068)
p85up	gcgGGATCCacc**ATG**agtgctgaggggtaccag	p85a(1-724)
p85down	cgGTCGAC**TTA**tcatcgcctctgctgtgcata	p85a(1-724)

Introduced restriction sites are in uppercase text; start and stop codons are in bold text.